Entropy Stable Discontinuous Galerkin Finite Element Method with Multi-Dimensional Slope Limitation for Euler Equations

Aziz Madrane[1], Fayssal Benkhaldoun[2]

Abstract. We present an entropy stable Discontinuous Galerkin (DG) finite element method to approximate systems of 2-dimensional symmetrizable conservation laws on unstructured grids. The scheme is constructed using a combination of entropy conservative fluxes and entropy-stable numerical dissipation operators. The method is designed to work on structured as well as on unstructured meshes. As solutions of hyperbolic conservation laws can develop discontinuities (shocks) in finite time, we include a multi-dimensional slope limitation step to suppress spurious oscillations in the vicinity of shocks. The numerical scheme has two steps: the first step is a finite element calculation which includes calculations of fluxes across the edges of the elements using 1-D entropy stable solver. The second step is a procedure of stabilization through a truly multi-dimensional slope limiter. We compared the Entropy Stable Scheme (ESS) versus Roe's solvers associated with entropy corrections and Osher's solver. The method is illustrated by computing solution of the two stationary problems: a regular shock reflection problem and a 2-D flow around a double ellipse at high Mach number.

[1] *Department of Mechanical Engineering, McGill University, Montreal, QC H3A 2T8, Canada*
e-mail: madrane99@hotmail.com.

[2]*LAGA, Université PARIS 13, 99 Avenue J. B. Clément 93430, Villetaneuse, France*
e-mail: fayssal@math.univ-paris13.fr (Corresponding Author).

1. Introduction

In this paper, we construct an entropy stable discontinuous Galerkin (DG) scheme for the system of ideal compressible Euler equations. As most conservation laws from applications, the entropy condition is an important property for the Euler system. It is highly desirable to design high order DG schemes to satisfy entropy stability. It is well known that a conservation law system has an entropy if and only if it is symmetrizable. Our discontinuous finite element method consists of two steps. We first (predictor) perform a finite element computation which includes calculation of the fluxes across the edges of the triangular elements using entropy stable solver to satisfy the entropy condition. In the second step, which can be viewed as a correction step, we then proceed to stabilize our method through a truly multidimensional slope limiter. We observe that the two steps are independent from each other, and the limitation process is distinct from the flux calculation, contributing to the originality of the method.

Many problems in Physics and Engineering are modeled in terms of nonlinear partial differential equations termed as systems of conservation laws. Examples for systems of conservation laws include the Euler equations of gas dynamics, the shallow water equations of oceanography, the magnetohydrodynamics (MHD) equations of plasma physics and equations of nonlinear elasticity [10]. Numerical schemes serve as one of the key tools in the study of systems of conservation laws. Finite volume schemes [12], [17] are one of the most popular design frameworks for robust numerical schemes. Higher-order spatial accuracy is obtained from a non-oscillatory piecewise polynomial reconstruction in each cell. Reconstruction procedures such as the second-order TVD [17], ENO [16] and WENO [33] are typically employed. An alternative to high-order finite volume methods is the discontinuous Galerkin finite element method [30, 22, 8, 1] as described below can also be viewed as finite volume method but its control volumes are the discretization cells themselves. It is an extension to the Euler equations, through a field by field decomposition, of the method developed for the scalar case and applied in reservoir simulation [7] and [6]. To stabilize solutions near flow-field discontinuities, considerable progress has been made on the development of multi-dimentional limiter on quadrilateral and triangular elements [1]. The following two issues related to practical applications have not been clearly answered

- How can non-physical solutions that are triggered by strong discontinuities and geometric singularities be avoided?
- How can discontinuous solutions be regularized on multi-dimensional high-order elements?

The present work aims at developing an algorithm that avoids non-physical solutions on arbitrary elements, based on the construction of entropy stable schemes for systems of conservation laws, introduced by Tadmor in [37]. The construction is based on two ingredients -(i) construction of an entropy conservative flux satisfying a discrete entropy equality, and (ii) addition of suitable dissipation operators to satisfy a discrete entropy inequality. First-order entropy stable schemes, in which the solution is assumed to be piecewise constant in the cells, have been extended by Madrane et al [25] and Ismail [20] for Euler equation on unstructured grids. High-order entropy conservative and entropy stable fluxes for unstructured grids were developed in [26]. Second-order TVD limiter based and arbitrary order TVB limiter based RKDG

schemes are also shown to converge [9] for scalar problems. It is also possible to obtain rigorous convergence results for linear symmetrizable systems [14]. There have been numerous contributions improving the framework in many other aspects. To name a few, entropy stable DG methods were devised for convection-diffusion equation [4], [5], [15], MHD equations [3], [23], gradient flow problems [34], [35], two-phase flow problems [31].

The rest of the paper is organized as follows. In Section 2 we briefly outline Euler equations. Section 3 introduce the entropy framework. In Section 4 we describe the discretization of the domain and introduce the general semi-discrete scheme for system of conservation laws, and the construction of entropy conservative and entropy stable fluxes. Section 5 discuss the construction of truly multi-dimensional limiter. The algorithm is explained in Section 6. Several two dimensional numerical results are presented in Section 7 to demonstrate the robustness of the proposed schemes. Concluding remarks are made in Section 8.

2. Governing equations :

We consider the conservative form of the Euler equations in eulerian coordinates :

$$\mathbf{U}_t + \mathbf{f}_1(\mathbf{U})_x + \mathbf{f}_2(\mathbf{U})_y = 0 \tag{2.1}$$

with $\mathbf{U} : \Omega \times \mathbb{R}_+ \to \mathbb{R}^m$ for some $\Omega \subset \mathbb{R}^2$. Defining $\mathbf{f}(\mathbf{U}) = (\mathbf{f}_1(\mathbf{U}), \mathbf{f}_2(\mathbf{U}))$, we say that (2.1) is *hyperbolic* if the matrix $\frac{d}{d\mathbf{U}}(\mathbf{f}(\mathbf{U}) \cdot \mathbf{n})$ has m real eigenvalues for all nonzero $\mathbf{n} \in \mathbb{R}^2$. A prototypical example for (2.1) are the Euler equations of gas dynamics:

$$\mathbf{U} = \begin{pmatrix} \rho \\ \rho u \\ \rho v \\ \rho E \end{pmatrix}, \qquad \mathbf{f}_1(\mathbf{U}) = \begin{pmatrix} \rho u \\ \rho u^2 + p \\ \rho u v \\ (\rho E + p)u \end{pmatrix}, \qquad \mathbf{f}_2(\mathbf{U}) = \begin{pmatrix} \rho v \\ \rho u v \\ \rho v^2 + p \\ (\rho E + p)v \end{pmatrix}. \tag{2.2}$$

Let ρ, u, v, p, E, c and M denote the density, velocity components, pressure, total energy per unit mass, speed of sound and Mach number. For a perfect gas, the pressure, the speed of sound and the Mach number are given by

$$p = (\gamma - 1)(\rho E - \frac{1}{2}\rho(u^2 + v^2)), \quad c = \sqrt{\frac{\gamma p}{\rho}}, \quad M = \frac{\sqrt{u^2 + v^2}}{c}. \tag{2.3}$$

where γ is the ratio of specific heats, is taken equal to 1.4 for air. We denote $\mathbf{u} = (u, v)$.

In the sequel, we consider domains of computation related to external flows around bodies; in Fig. (1) the body is represented by a double-ellipse [19] which limits the domain of computation by its wall $\Gamma_{Wall} = \Gamma_B$. In order to deal with a bounded computational domain, a second (artificial) farfield boundary $\Gamma_\infty \cup \Gamma_S$ is introduced, with $\Gamma_S = \Gamma_S^1 \cup \Gamma_S^2 = \Gamma_{exit}$.
The flow is assumed to be uniform at farfield boudary $\Gamma_\infty \cup \Gamma_S$, and we prescribe

$$\rho_\infty = 1, \quad V_\infty = \begin{pmatrix} cos\alpha \\ sin\alpha \end{pmatrix}, \quad p_\infty = \frac{1}{\gamma M_\infty^2} \tag{2.4}$$

where α is the angle of attack and M_∞ denotes the free-stream Mach number.
On the wall Γ_B we use the usual "no normal velocity" condition: $\vec{V}.\vec{n} = 0$, where $\vec{n} \in R^2$ is the outer normal vector to Γ_B.
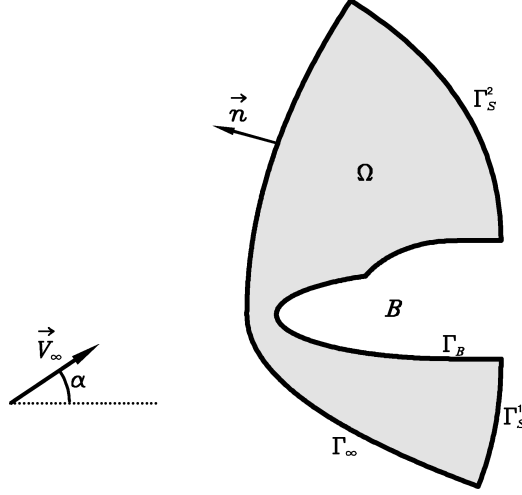
FIGURE 1. Flow past a double ellipse at high angle of attack: the problem definition and the computational domain (shaded)

Finally, for unsteady calculations, an initial flow is prescribed :

$$U(x, y; 0) = U_0(x, y) \quad \forall (x, y) \in \Omega. \tag{2.5}$$

3. Entropy framework

The solutions of (2.1) may develop discontinuities in finite time when even the initial data is smooth. Hence, solutions of (2.1) are sought in the sense of distributions. Additional admissibility criteria need to be imposed to single out unique solutions. Such criteria, called *entropy conditions*, rely on the existence of a convex function η and functions q_1, q_2 such that the following compatibility conditions hold:

$$q_1'(\mathbf{U})^\top = \eta'(\mathbf{U})^\top \mathbf{f}_1'(\mathbf{U}), \qquad q_2'(\mathbf{U})^\top = \eta'(\mathbf{U})^\top \mathbf{f}_2'(\mathbf{U}). \tag{3.1}$$

It is straightforward to check using (3.1) that *smooth* solutions of (2.1) satisfy an additional conservation law, the entropy identity

$$\eta(\mathbf{U})_t + q_1(\mathbf{U})_x + q_2(\mathbf{U})_y = 0. \tag{3.2}$$

However, entropy needs to be dissipated at shocks. Hence, the entropy identity (3.2) is replaced by an entropy inequality,

$$\eta(\mathbf{U})_t + q_1(\mathbf{U})_x + q_2(\mathbf{U})_y \leq 0, \tag{3.3}$$

that holds in the sense of distributions. The vector $\mathbf{V} = \eta'(\mathbf{U})$ is termed as the vector of *entropy variables*. The entropy inequality (3.3) is integrated in space to yield the stability estimate

$$\frac{d}{dt} \int_{\mathbb{R}^2} \eta(\mathbf{U}(x, y, t)) dx dy \leq 0. \tag{3.4}$$

Given the strict convexity of the entropy function, the entropy framework through (3.4) provides an a priori L^2 stability estimate for the mult-dimensional system (2.1)

We illustrate the entropy framework for the Euler equations (2.2). Define the standard logarithmic entropy $s := \log(p) - \gamma \log(\rho)$. Then the couple entropy function- entropy fluxes $(\eta(\mathbf{U}), q(\mathbf{U}))$ for the Euler equations are given by

$$\eta(\mathbf{U}) = -\frac{\rho s}{\gamma - 1}, \quad q(\mathbf{U}) = \begin{pmatrix} q_1(\mathbf{U}) = -\frac{\rho u s}{\gamma - 1}, \\ q_2(\mathbf{U}) = -\frac{\rho v s}{\gamma - 1} \end{pmatrix}. \tag{3.5}$$

Note that this mathematical entropy is the opposite of the physical entropy of Euler system. The entropy variable $\mathbf{V} = (v_1, v_2, v_3, v_4)^\top$ associated with $\eta(\mathbf{U})$ is given by

$$\mathbf{V}(\mathbf{U}) = \left(\frac{\gamma - s}{\gamma - 1} - \frac{\rho |\mathbf{u}|^2}{p}, \frac{\rho u}{p}, \frac{\rho v}{p}, -\frac{\rho}{p} \right)^\top. \tag{3.6}$$

The inverse mapping $\mathbf{V} \to \mathbf{U}(\mathbf{V})$ is given by (the conservation variables in terms of the entropy variables)

$$\mathbf{U}(\mathbf{V}) = \left(\rho = -p v_4, \quad \rho u = p v_2, \quad \rho v = p v_3, \quad \rho E = p \left(\frac{1}{(\gamma - 1)} - \frac{v_2^2 + v_3^2}{2 v_4} \right) \right)^\top \tag{3.7}$$

where p and s in terms of the entropy variables are

$$p = (-v_4)^{\frac{\gamma}{1-\gamma}} (\exp(-s))^{\frac{1}{\gamma-1}}, \quad s = \gamma - (\gamma - 1) \left(v_1 - \frac{v_2^2 + v_3^2}{2 v_4} \right) \tag{3.8}$$

Note that the first component of $\mathbf{U}(\mathbf{V})$ (i.e. ρ) is positive by construction.

3.1. Symmetrization: The results of Godunov and Mock show that a hyperbolic system (2.1) is symmetrizable if and only if it has an entropy framework. A particularly revealing form of this symmetrization is due to Barth [2]. The key to this symmetrized form is a theorem of [2] showing that for every nonzero $\mathbf{n} \in \mathbb{R}^2$, there exist suitably scaled matrix of eigenvectors $R_\mathbf{n}$ of the matrix $\frac{d}{d\mathbf{U}}(\mathbf{f}(\mathbf{U}) \cdot \mathbf{n})$ such that

$$R_\mathbf{n} R_\mathbf{n}^\top = \mathbf{U_V}, \tag{3.9}$$

with $\mathbf{U_V} = \mathbf{U}'(\mathbf{V})$ being the change-of-variables matrix from the conserved variables $\mathbf{U}$ to the entropy variables $\mathbf{V}$. This identity is independent of the direction $\mathbf{n}$, thus providing a natural scaling for the eigenvectors. Denote $R_k = R_{\mathbf{e}_k}$, with $\mathbf{e}_k$ being the unit vector in direction k, and let Λ_k be the corresponding diagonal matrix of eigenvalues. Using (3.9), we formally obtain

$$\begin{aligned} \mathbf{U}_t + \mathbf{f}_1(\mathbf{U})_x + \mathbf{f}_2(\mathbf{U})_y &= \mathbf{U}(\mathbf{V})_t + \mathbf{f}_1(\mathbf{U}(\mathbf{V}))_x + \mathbf{f}_2(\mathbf{U}(\mathbf{V}))_y, \\ &= \mathbf{U}_t + \mathbf{f}_1'(\mathbf{U})\mathbf{U}_x + \mathbf{f}_2'(\mathbf{U})\mathbf{U}_y, \\ &= \mathbf{U_V}\mathbf{V}_t + R_1 \Lambda_1 R_1^{-1} \mathbf{U_V}\mathbf{V}_x + R_2 \Lambda_2 R_2^{-1} \mathbf{U_V}\mathbf{V}_y, \\ &= \mathbf{U_V}\mathbf{V}_t + R_1 \Lambda_1 R_1^\top \mathbf{V}_x + R_2 \Lambda_2 R_2^\top \mathbf{V}_y. \end{aligned} \tag{3.10}$$

As η is a convex function, $\mathbf{U_V}$ is a symmetric positive definite matrix. Clearly the coefficient matrices $R_k \Lambda_k R_k^\top$ for $k = 1, 2$ are symmetric, implying that the conservation law (2.1) has the symmetrized form

$$\mathbf{U_V}\mathbf{V}_t + R_1 \Lambda_1 R_1^\top \mathbf{V}_x + R_2 \Lambda_2 R_2^\top \mathbf{V}_y = 0. \tag{3.11}$$

For the Euler equations with the aforementioned entropy function, the change of variables matrix is given by

$$\mathbf{U_V} = \begin{pmatrix} \rho & \rho \mathbf{u}^\top & E \\ \rho \mathbf{u} & \rho \mathbf{u} \mathbf{u}^\top + p\mathbf{I} & \rho H \mathbf{u} \\ E & \rho H \mathbf{u}^\top & \rho H^2 - \frac{c^2 p}{\gamma - 1} \end{pmatrix}$$

where the specific enthalpy is $H = \frac{c^2}{\gamma - 1} + \frac{|\mathbf{u}|^2}{2}$. The resulting scaled eigenvectors are

$$r_\mathbf{n}^1 = \sqrt{\frac{\rho(\gamma - 1)}{\gamma}} \left(n_1, \; un_1, \; vn_1, \; \frac{(u^2 + v^2)n_1}{2} \right)^\top,$$

$$r_\mathbf{n}^2 = \sqrt{\frac{\rho(\gamma - 1)}{\gamma}} \left(0, \; -\frac{cn_2}{\sqrt{\gamma - 1}}, \; \frac{cn_1}{\sqrt{\gamma - 1}}, \; -\frac{(vn_1 - un_2)c}{\sqrt{\gamma - 1}} \right)^\top,$$

$$r_\mathbf{n}^3 = \sqrt{\frac{\rho}{2\gamma}} \left(1, \; u + cn_1, \; v + cn_2, \; H + c(un_1 + vn_2) \right)^\top,$$

$$r_\mathbf{n}^4 = \sqrt{\frac{\rho}{2\gamma}} \left(1, \; u - cn_1, \; v - cn_2, \; H - c(un_1 + vn_2) \right)^\top. \tag{3.12}$$

The diagonal matrix of eigenvalues is given by

$$\Lambda_\mathbf{n} = \text{diag}\left(un_1 + vn_2, \; un_1 + vn_2, \; un_1 + vn_2 + c, \; un_1 + vn_2 - c \right). \tag{3.13}$$

In the following section we describe how to derive an efficient method to solve these equations by using a discontinuous finite element approximation.

4. A two-dimensional discontinuous Galerkin method

4.1. Preliminaries. The computational domain Ω is subdivided into triangles or quadrangles by a triangulation $\mathcal{T}_h$:

$$\Omega = \bigcup_{i=1}^{N_e} K_i \; ; \; K_i \in \mathcal{T}_h,$$

where the K_i's are the elements of the triangulation, N_e is the total number of elements, and h is the largest diameter of all elements. We use the linear and quadratic basic function in triangular and quadrilateral partition, which is defined as follows:

$$\begin{cases} P^1(K_i), & \text{if } K_i \text{ is a triangle} \\ Q^1(K_i), & \text{if } K_i \text{ is a quadrangle} \end{cases}$$

Let $\mathbf{U}_{l,i} = \mathbf{U}(A_{l,i}; t)$ denote the value of the dependent variable vector $\mathbf{U}$, at time t and at the lth vertex $A_{l,i}$ of element $K_i \in \mathcal{T}_h$ ($i = 1, \ldots, N_e; l = 1, \ldots, nv(K)$), $nv(K)$number of vertices of $K_,$.

The degrees of freedom are the components of the vector $\mathbf{U}$ at the vertices of all elements of the triangulation Fig. (2).
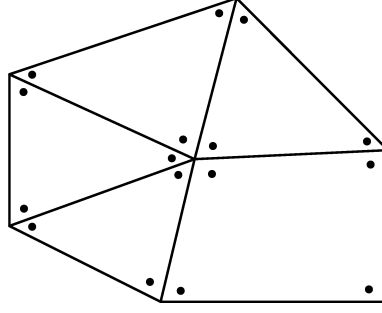
FIGURE 2. Degrees of freedom of discretization

Let W denote the approximation space formed by the piecewise continuous functions which are linear on each triangle $K_i \in \mathcal{T}_h$,

$$W = \left\{ U/U_K \in \left| \begin{array}{ll} P^1(K), & \text{if } K \text{ is a triangle} \\ Q^1(K), & \text{if } K \text{ is a quadrangle} \end{array} \right. ; K \in \mathcal{T}_h \right\}$$

The vector $\mathbf{U}$ of conservative variables ρ, ρu, ρv, ρE is approximated by functions in the product space W^4 and the corresponding approximations will again be denoted by ρ, ρu, ρv, ρE, elements of W, for simplicity.

For each element $K_i(i = 1, \ldots, N_e)$ and each node $A_{l,i} \in K_i$ there exists a unique basis or shape function $(\varphi_{l,i})$ with the property

$$\forall \, i = 1, \ldots, N_e \, , \quad \varphi_{l,i}(A_{k,i}) = \left\{ \begin{array}{ll} 1 & \text{if } l = k \\ 0 & \text{otherwise} \end{array} \right.$$

The functions $(\varphi_{l,i})_{i=1,\ldots,N_e}^{l=1,\ldots,nv(K)}$ form a basis of the approximation space W.

In the present formulation we shall use an explicit Euler time discretization.

4.2. The DG method with entropy variables. We now consider a Galerkin discontinuous finite element approximation, which proceeds from a variational formulation of the Euler equations. Here, we have used the change of variable $\mathbf{U} = \mathbf{U}(\mathbf{V})$ and retained the notation $\mathbf{f}_k(\mathbf{U}) = \mathbf{f}_k(\mathbf{U}(\mathbf{V}))$ for all k for notation convenience. Following [2, 37], we approximate the conservation law (3.10) by a DG method.

Multiplying (3.10) by a shape function $\varphi_{l,i}$ and integrating by parts the terms with spatial derivatives, we obtain the following system for the piecewise linear vector $\mathbf{U}^{n+1}$ of approximate dependent variables to be computed at time t^{n+1}:

$$\left\{ \begin{array}{l} \text{Find } \mathbf{U}^{n+1} \in W^4 \\ \\ \int_{K_i} \dfrac{\mathbf{U}^{n+1} - \mathbf{U}^n}{\Delta t^n} \varphi_{l,i} \, dS = \int_{K_i} \left(\mathbf{f}_1(\mathbf{U}^n) \dfrac{\partial \varphi_{l,i}}{\partial x} + \mathbf{f}_2(\mathbf{U}^n) \dfrac{\partial \varphi_{l,i}}{\partial y} \right) dS - \int_{\partial K_i} (\mathbf{f}(U^n) \cdot \boldsymbol{n}) \, \varphi_{l,i} \, d\sigma \end{array} \right. \tag{4.1}$$

where $\Delta t^n = t^{n+1} - t^n$ is the time step, $\mathbf{U}^n = \mathbf{U}(x,y;t^n) \in W^4$, and $\boldsymbol{n} = \begin{pmatrix} n^1 \\ n^2 \end{pmatrix}$ is the unit outer normal (directed towards the exterior of K_i).

In (4.1), $\mathbf{f}(\mathbf{U}^n) \cdot \mathbf{n} = \mathbf{f}_1(\mathbf{U}^n) \cdot n^1 + \mathbf{f}_2(\mathbf{U}^n) \cdot n^2 \equiv \mathbf{f}_n$ is the (outward) numerical flux across an edge $\mathcal{A}$ of ∂K_i; it will be computed with the help of an approximate Riemann solver for the Riemann problem generated, in the direction normal to the edge $\mathcal{A}$, by the limits of the values of the dependent variables on both sides of $\mathcal{A}$ as one tends to $\mathcal{A}$ along $\vec{n}$.

In this paper, we have used Osher's Riemann solver [27], Roe's Riemann solver [32] with an entropic correction due to Madrane and Tadmor [24] and entropy stable scheme [25].

Remark 1. *Replacing the above approximation space by the space of piecewise constant functions (constant on each triangle $K_i \in \mathcal{T}_h$) reduces (4.1) to the equation governing the standard finite volume scheme, which is a first order scheme in space, so that the solutions are located at the element's center.*

$$\int_{K_i} \frac{\mathbf{U}_i^{n+1} - \mathbf{U}_i^n}{\Delta t^n} \, dS + \int_{\partial K_i} (\mathbf{f}(\mathbf{U}^n) \cdot \mathbf{n}) \, d\sigma = 0, \quad K_i \in \mathcal{T}_h.$$

4.3. Numerical integration. To complete the description of the spatial discretization, we must specify the quadrature formulas which will be used to compute the integrals appearing in (4.1). Numerical experiments for scalar equation [18] have suggested the following quadrature techniques that are first order in space.

In equation (4.1) the terms containing the spatial derivatives are computed with the help of the values at the centroid M of mesh K_i:

$$\int_{K_i} \left(\mathbf{f}_1(\mathbf{U}^n) \frac{\partial \varphi_{l,i}}{\partial x} + \mathbf{f}_2(\mathbf{U}^n) \frac{\partial \varphi_{l,i}}{\partial y} \right) dS \simeq \text{Area}(K_i) \left(\mathbf{f}_1(\overline{\mathbf{U}}_i^n) \frac{\partial \varphi_{l,i}}{\partial x}(M_i) + \mathbf{f}_2(\overline{\mathbf{U}}_i^n) \frac{\partial \varphi_{l,i}}{\partial y}(M_i) \right) \quad (4.2)$$

where M_i is the centroid of K_i and $\overline{\mathbf{U}}_i^n$ is the average value of $\mathbf{U}^n$ on K_i :

$$\overline{\mathbf{U}}_i^n = \frac{1}{nv(K_i)} \sum_{l=1}^{nv(K)} \mathbf{U}(A_{l,i})$$

since $\mathbf{U}^n$ is linear on K_i.

For the integral associated with the outward flux

$$\int_{\partial K_i} (\mathbf{f}(\mathbf{U}^n) \cdot \mathbf{n}) \, \varphi_{l,i} \, d\sigma = \sum_{\mathcal{A} \in \partial K_i} \int_{\mathcal{A}} (\mathbf{f}(\mathbf{U}^n) \cdot \mathbf{n}) \, \varphi_{l,i} \, d\sigma$$

we use either the values at the midpoints of the edges $\mathcal{A}$, or the values at both Gauss points of each edge
1st choice :

$$\int_{\mathcal{A}} (\mathbf{f}(\mathbf{U}^n) \cdot \mathbf{n}) \, \varphi_{l,i} \, d\sigma \simeq l(\mathcal{A}) \cdot \mathcal{F}_{|\mathcal{A}}(\mathbf{U}_i^n, \mathbf{U}_j^n, \mathbf{n}_{ij}) \cdot \varphi_{l,i}(M)$$

where $l(\mathcal{A})$ and M denote the length and midpoint of edge $\mathcal{A}$, respectively, and $\mathcal{F}_{|\mathcal{A}}(\mathbf{U}_i^n, \mathbf{U}_j^n, \mathbf{n}_{ij}) = \mathbf{F}_{ij}$ is the <u>numerical flux</u> across edge $\mathcal{A}$ which separates the states $\mathbf{U}_i$ and $\mathbf{U}_j$, obtained by taking the limits of $\mathbf{U}$ along the normal to $\mathcal{A}$ at M see Fig. (3); this numerical flux will be computed with Riemann solver, as described below.
2nd choice :

$$\int_{\mathcal{A}} (\mathbf{f}(\mathbf{U}^n) \cdot \mathbf{n}) \, \varphi_{l,i} \, d\sigma \simeq \frac{l(\mathcal{A})}{2} \left(\mathcal{F}_{|_{\mathcal{A}}}(\mathbf{U}_i^n, \mathbf{U}_j^n, \mathbf{n}_{ij})(G_1)\varphi_{l,i}(G_1) + \mathcal{F}_{|_{\mathcal{A}}}(\mathbf{U}_i^n, \mathbf{U}_j^n, \mathbf{n}_{ij})(G_2)\varphi_{l,i}(G_2) \right)$$

(4.3)

where G_1, G_2 are the Gauss points of edge $\mathcal{A}$.

Numerical experiments have shown that the computation at the edge midpoint (1st choice) is sufficient.

For the first integral in (4.1) (time derivative) we use the values at the three vertices:

$$\int_{K_i} \frac{\mathbf{U}^{n+1} - \mathbf{U}^n}{\Delta t^n} \varphi_{l,i} \, dS \simeq \frac{\text{Area}(K_i)}{nv(K_i)} \frac{\mathbf{U}_{K_i,A_l}^{n+1} - \mathbf{U}_{K_i,A_l}^n}{\Delta t^n}$$
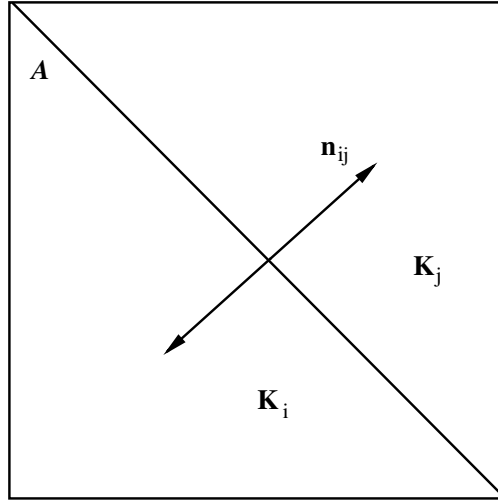
by the properties of $\varphi_{l,i}$.

FIGURE 3. Two elements K_i and K_j sharing edge $\mathcal{A}$.

Remark 2. *The spatial numerical flux is assumed to be conservative, i.e.*

$$\mathcal{F}_{|_{\mathcal{A}}}(a, b, \mathbf{n}) = \mathcal{F}_{|_{\mathcal{A}}}(b, a, -\mathbf{n})$$

(4.4)

for all directions $\mathbf{n}$ and all states a and b, and consistent, i.e.

$$\mathcal{F}_{|_{\mathcal{A}}}(a, a, \mathbf{n}) = \mathbf{f}(a) \cdot \mathbf{n} = \mathbf{f}_1(a) \cdot n^1 + \mathbf{f}_2(a) \cdot n^2 \equiv \mathbf{f}_n$$

(4.5)

for all directions $\mathbf{n}$ and all states a.

4.4. Entropy conservative flux for Euler equations. We aim to design a numerical flux such that the resulting numerical scheme (6.1) is *entropy conservative* i.e, it satisfies a discrete version of the entropy identity (3.2). The concept of entropy conservative schemes for systems of conservation laws was introduced by Tadmor in [36] for Cartesian meshes. In this section we extend the notion of entropy conservative schemes to unstructured meshes.

Definition 4.1. *A numerical flux* $\widetilde{\mathbf{F}}_{ij} = \widetilde{\mathbf{F}}_{ij}^1 n_{ij}^1 + \widetilde{\mathbf{F}}_{ij}^2 n_{ij}^2$ *is* entropy conservative *if*

$$[\![\mathbf{V}]\!]_{ij}^\top \widetilde{\mathbf{F}}_{ij} = \psi(\mathbf{U}_j, n_{ij}) - \psi(\mathbf{U}_i, n_{ij}), \tag{4.6}$$

where $\psi(\mathbf{U}, n) = \mathbf{V}(\mathbf{U})^\top \mathbf{f}(\mathbf{U}, n) - q(\mathbf{U}, n)$ *denotes the entropy potential and* $q(\mathbf{U}, n) = q_1(\mathbf{U})n^1 + q_2(\mathbf{U})n^2$.

We note that the condition (4.6) provides a single algebraic equation for m unknowns. In general, it is not clear whether a solution of (4.6) exists. Furthermore, the solutions of (4.6) will not be unique except for scalar equations. In [36], Tadmor showed the existence of at least one solution of (4.6) for any system of conservation laws. Explicit solutions were constructed in [37]. However, the entropy conservative fluxes of [37] are computationally expensive; see [13]. Instead, we follow recent papers [25, 13, 20] to obtain algebraically simple and computational inexpensive solution of (4.6). For concreteness we consider the Euler equations of gas dynamics (2.2). Denote by Z the so-called Roe parameter vector

$$Z = \sqrt{\frac{\rho}{p}} \begin{pmatrix} 1 \\ u \\ v \\ p \end{pmatrix}.$$

It is readily verified that

$$\rho = Z_1 Z_4, \quad p = \frac{Z_4}{Z_1}, \quad u = \frac{Z_2}{Z_1}, \quad v = \frac{Z_3}{Z_1}, \quad m_1 = \rho u = Z_2 Z_4, \quad m_2 = \rho v = Z_3 Z_4$$

Denoting by $s = \log(p) - \gamma \log(\rho)$ the standard logarithmic entropy, we have

$$s = \ln\left(\frac{Z_4^{(1-\gamma)}}{Z_1^{(1+\gamma)}}\right), \qquad \eta(\mathbf{U}) = \frac{-Z_1 Z_4 s}{\gamma - 1}.$$

The entropy variables are

$$\mathbf{V} = \begin{pmatrix} \frac{\gamma - s}{\gamma - 1} - \frac{m_1^2 + m_2^2}{2p\rho} \\ \frac{m_1}{p} \\ \frac{m_2}{p} \\ -\frac{\rho}{p} \end{pmatrix} = \begin{pmatrix} \frac{\gamma}{\gamma - 1} + \ln(Z_4) + \left(\frac{1+\gamma}{1-\gamma}\right)\ln Z_1 - \frac{Z_2^2 + Z_3^2}{2} \\ Z_1 Z_2 \\ Z_1 Z_3 \\ -Z_1^2 \end{pmatrix},$$

the entropy fluxes are

$$q_1(\mathbf{U}) = \frac{-m_1 s}{\gamma - 1} = \frac{-Z_2 Z_4 s}{\gamma - 1}, \qquad q_2(\mathbf{U}) = \frac{-m_2 s}{\gamma - 1} = \frac{-Z_3 Z_4 s}{\gamma - 1}$$

and the entropy potentials are

$$\psi_1(\mathbf{U}) = m_1, \qquad \psi_2(\mathbf{U}) = m_2. \tag{4.7}$$

Using the jump identity $[\![ab]\!] = \bar{a}[\![b]\!] + \bar{b}[\![a]\!]$ for Eq. 4.7 we obtain $[\psi_1(\mathbf{U})] = \overline{Z_2}[\![Z_4]\!] + \overline{Z_4}[\![Z_2]\!]$ and $[\psi_2(\mathbf{U})] = \overline{Z_3}[\![Z_4]\!] + \overline{Z_4}[\![Z_3]\!]$, respectively. Where $[\![a]\!]_{ij} = a_i - a_j, \quad \bar{a}_{ij} = (a_i + a_j)/2$.

Let $\widetilde{\mathbf{F}}_1 = \left(\widetilde{\mathbf{F}}_1^1, \widetilde{\mathbf{F}}_1^2, \widetilde{\mathbf{F}}_1^3, \widetilde{\mathbf{F}}_1^4\right)^\top$, be an entropy conservative flux and $\mathbf{V} = (v_1, v_2, v_3, v_4)^\top$, then Eq. 4.6 result in,

$$\widetilde{\mathbf{F}}_1^1[\![v_1]\!] + \widetilde{\mathbf{F}}_2^1[\![v_2]\!] + \widetilde{\mathbf{F}}_3^1[\![v_3]\!] + \widetilde{\mathbf{F}}_4^1[\![v_4]\!] = [\psi_1(\mathbf{U})]$$

which simplifies to

$$\widetilde{F}_1^1\left(\frac{[\![Z_4]\!]}{Z_4^{\ln}} + \frac{\gamma+1}{\gamma-1}\frac{[\![Z_1]\!]}{Z_1^{\ln}} - \bar{Z}_2[\![Z_2]\!] - \bar{Z}_2[\![Z_2]\!]\right) + \widetilde{F}_1^2[\![Z_1 Z_2]\!] + \widetilde{F}_1^3[\![Z_1 Z_3]\!] - \widetilde{F}_1^4\left[\!\left[Z_1^2\right]\!\right] - [\![Z_2 Z_4]\!] = 0$$

by equating jumps in the same variables, we obtain $\widetilde{\mathbf{F}}_1 = \left(\widetilde{\mathbf{F}}_1^1, \widetilde{\mathbf{F}}_1^2, \widetilde{\mathbf{F}}_1^3, \widetilde{\mathbf{F}}_1^4\right)^\top$, where the components are given by

$$\widetilde{\mathbf{F}}_1 = \begin{pmatrix} \widetilde{\mathbf{F}}_1^1 \\ \widetilde{\mathbf{F}}_1^2 \\ \widetilde{\mathbf{F}}_1^3 \\ \widetilde{\mathbf{F}}_1^4 \end{pmatrix} = \begin{pmatrix} \dfrac{\overline{Z_2}Z_4^{\ln}}{\overline{Z_4}+\widetilde{F}_1^1\overline{Z_2}} \\ \dfrac{\overline{Z_1}}{\overline{Z_1}} \\ \dfrac{\overline{Z_2 Z_3}Z_2^{\ln}}{\overline{Z_1}} \\ \dfrac{\frac{\gamma+1}{\gamma-1}\frac{1}{Z_1^{\ln}}\widetilde{F}_1^1 + \overline{Z_2}\widetilde{F}_1^2 + \overline{Z_3}\widetilde{F}_1^3}{2\overline{Z_1}} \end{pmatrix}$$

Similarly, we can derive the expression for $\widetilde{\mathbf{F}}_2$ given by

$$\widetilde{\mathbf{F}}_2 = \begin{pmatrix} \widetilde{\mathbf{F}}_2^1 \\ \widetilde{\mathbf{F}}_2^2 \\ \widetilde{\mathbf{F}}_2^3 \\ \widetilde{\mathbf{F}}_2^4 \end{pmatrix} = \begin{pmatrix} \dfrac{\overline{Z_3}Z_4^{\ln}}{\overline{Z_2}\widetilde{F}_2^1} \\ \dfrac{\overline{Z_1}}{\overline{Z_1}} \\ \dfrac{\overline{Z_4}+\widetilde{F}_2^1\overline{Z_3}}{\overline{Z_1}} \\ \dfrac{\frac{\gamma+1}{\gamma-1}\frac{1}{Z_1^{\ln}}\widetilde{F}_2^1 + \overline{Z_2}\widetilde{F}_2^2 + \overline{Z_3}\widetilde{F}_2^3}{2\overline{Z_1}} \end{pmatrix}.$$

Here, $a^{\ln}$ is the logarithmic mean defined as

$$a^{\ln} = \frac{[\![a]\!]}{[\log(a)]},$$

See [20] for further details.

The multi-dimensional entropy conservative flux in terms of Z can be written as follows:

$$\mathbf{F}_{ij} = \quad \widetilde{\mathbf{F}}(\mathbf{Z}_{ij}, t^n) \cdot \vec{\mathbf{n}}_{ij} = \begin{pmatrix} \widetilde{\mathbf{F}}^\rho \\ \widetilde{\mathbf{F}}^{\rho u} \\ \widetilde{\mathbf{F}}^{\rho v} \\ \widetilde{\mathbf{F}}^e \end{pmatrix} = \begin{pmatrix} \dfrac{\widetilde{\mathbf{Z}}_{ij}Z_4^{\ln}}{\overline{\mathbf{Z}_1}}\mathbf{n}_{ij}^1 + \dfrac{\overline{\mathbf{Z}_2}}{\overline{\mathbf{Z}_1}}\widetilde{\mathbf{F}}^\rho \\ \dfrac{\overline{\mathbf{Z}_4}}{\overline{\mathbf{Z}_1}}\mathbf{n}_{ij}^2 + \dfrac{\overline{\mathbf{Z}_3}}{\overline{\mathbf{Z}_1}}\widetilde{\mathbf{F}}^\rho \\ \dfrac{1}{2\overline{\mathbf{Z}_1}}\left[\dfrac{(\gamma+1)}{(\gamma-1)}\dfrac{\widetilde{\mathbf{F}}^\rho}{Z_1^{\ln}} + \overline{\mathbf{Z}_2}\widetilde{\mathbf{F}}^{\rho u} + \bar{\mathbf{Z}}_3\widetilde{\mathbf{F}}^{\rho v}\right] \end{pmatrix} \tag{4.8}$$

Where

$$\widetilde{\mathbf{Z}}_{ij} = \overline{\mathbf{Z}}_2 \mathbf{n}_{ij}^1 + \overline{\mathbf{Z}}_3 \mathbf{n}_{ij}^2$$

4.5. Entropy stable flux for Euler equations.

4.5.1. *Numerical diffusion operators.* The entropy conservative schemes lead to unphysical oscillations near shocks. We need to add numerical diffusion to eliminate these oscillations. Following the procedure of [25], we consider numerical flux functions

$$\mathbf{F}_{ij} = \widetilde{\mathbf{F}}_{ij} - \frac{1}{2} \mathbf{D}_{ij} [\![\mathbf{V}]\!]_{ij}. \tag{4.9}$$

Here, $\widetilde{\mathbf{F}}$ is an entropy conservative flux and $\mathbf{D}$ is any symmetric positive definite matrix with $\mathbf{D}_{ij} = \mathbf{D}_{ji}$.

We impose the following additional conditions on the entropy-conservative flux to obtain a consistent (4.5) and conservative (4.4) numerical flux. The entropy-conservative flux itself should be consistent, i.e.

$$\widetilde{\mathbf{F}}^k(a, a) = \mathbf{F}^k(a) \tag{4.10}$$

for all k and all states a, and symmetric, i.e.

$$\widetilde{\mathbf{F}}^k(a, b) = \widetilde{\mathbf{F}}^k(b, a) \tag{4.11}$$

for all k and all states a and b. One could drop the symmetry requirement, but then $\widetilde{\mathbf{F}}^k$ would need to depend on the normal n in order to obtain a conservative flux.

The flux $\mathbf{F}_{ij}$ is consistent this implies that $\mathbf{F}(\mathbf{U}_i, \mathbf{U}_i) = \widetilde{\mathbf{F}}(\mathbf{U}_i, U_i) - 0 = \mathbf{f}(U_i) \cdot \mathbf{n}_i$, and it is conservative because $\mathbf{F}_{ji} = \widetilde{\mathbf{F}}_{ji} - \frac{1}{2} \mathbf{D}_{ji} \left(-[\![\mathbf{V}]\!]_{ij} \right) = \left(\widetilde{\mathbf{F}}_{ij} - \frac{1}{2} \mathbf{D}_{ij} [\![\mathbf{V}]\!]_{ij} \right) = \mathbf{F}_{ij}$.

4.5.2. *Specifying the numerical diffusion matrix.* Following [25], we choose the numerical diffusion operator as,

$$\mathbf{D}_{ij} = R_{\mathbf{n}_{ij}} P(\Lambda_{\mathbf{n}_{ij}}) R_{\mathbf{n}_{ij}}^\top. \tag{4.12}$$

Here, $\Lambda_{\mathbf{n}}$ and $R_{\mathbf{n}}$ are the matrix of eigenvalues and eigenvectors of the Jacobian matrix $\frac{d}{d\mathbf{U}}(\mathbf{f}(\mathbf{U}) \cdot \mathbf{n})$ in the normal direction $\mathbf{n}$. $R_{\mathbf{n}}$ is evaluated at an averaged state, e.g. $(\mathbf{U}_i + \mathbf{U}_j)/2$. Example of P include $P(\Lambda_{\mathbf{n}_{ij}}) = |\Lambda_{\mathbf{n}_{ij}}(\mathbf{U}_i + \mathbf{U}_j)/2|$ which leads to a Roe type scheme.

4.6. Note on the implementation of the time discretization.
In this paper, we limit our applications to the computation of stationary solutions, and will therefore use a local time stepping process described below.

Introducing the diagonal matrix $\Sigma = \text{diag} \left[\dfrac{\text{Area}(K_i)}{\Delta t_i^n} \right]_{K_i \in \mathcal{T}_h}$, we can write (6.1) as follows:

$$\begin{cases} \text{Find } \mathbf{U}^\star \in W^4 \quad \text{such that} \\ \\ \mathbf{U}^\star - \mathbf{U}^n = -\Sigma^{-1} \, \mathcal{R}(U^n) \end{cases} \tag{4.13}$$

where $\mathcal{R}(U^n)$ is the residual defined from the right-hand side of (6.1)

$$\mathcal{R}(\mathbf{U}^n) = \int_{\partial K_i} (\mathbf{f}(\mathbf{U}^n) \cdot \boldsymbol{n}) \, \varphi_{l,i} \, d\sigma \ - \ \int_{K_i} \left(\mathbf{f}_1(\mathbf{U}^n) \frac{\partial \varphi_{l,i}}{\partial x} + \mathbf{f}_2(\mathbf{U}^n) \frac{\partial \varphi_{l,i}}{\partial y} \right) \, dS \, . \qquad (4.14)$$

The scheme (4.13) is stable under an appropriate $CFL - condition$.

Let μ denote the $CFL - number$ (assumed to be uniform on the whole grid). For each element $K_i \in \mathcal{T}_h$ we note

- ν_i : mean value, in element K_i, of the characteristic speed corresponding to the largest eigenvalue

$$\nu_i = \sqrt{\overline{u_i^2} + \overline{v_i^2}} + \overline{c}_i \, ,$$

- h_i : ratio of the area of K_i by its perimeter

$$h_i = \frac{\text{Area}(K_i)}{\text{L}(K_i)} \, .$$

The local time step is then chosen so that

$$\Delta t_i^n \leq \mu \frac{h_i}{\nu_i} . \qquad (4.15)$$

In most cases we have used a $CFL - number \ \mu = 0.5$.

5. Multi-dimensional slope limitation strategy

We will describe a multi-dimensional extension of a slope limitation procedure which has been successfully used for scalar equations [18].

When dealing with the Euler equations, it has been widely recognized that one should limit the physical variables ρ, u, v, p rather than the conservative variables ρ, ρu, ρv, ρE.

Let $\mathbf{U}^n \in W^4$ denote the solution previously computed at time t^n, and $\mathbf{U}^\star \in W^4$ the solution predicted at t^{n+1} by solving system (4.1).

We want to modify $\mathbf{U}^\star$ and obtain a corrected vector of conservative variables $\mathbf{U}^{n+1}$, by the following procedure.

For each triangle $K_i \in \mathcal{T}_h$, let

- $nv(K)$number of vertices of K,
- $w_{K,A_i} = w_{|K}(A_i) : \quad i = 1, \ldots, nv(K) \quad$ be the value of $w_{|K}$ at node i,
- $\overline{w}_K = \dfrac{1}{nv(K)} \displaystyle\sum_{i=1}^{nv(K)} w_{K,A_i}$, the mean value of $w_{|K}$ in element K,
- $T(A)$ be the set of element $K \in \mathcal{T}_h$ such that vertex $A \in K$.

For each element K, we compute the mean values of the conservative variables, noted $\overline{\rho}_K^\star$, $\overline{(\rho u)}_K^\star$, $\overline{(\rho v)}_K^\star$, $\overline{(\rho E)}_K^\star$,which are simply the arithmetic means of these variables at the three vertices of K.

In order to obtain a conservative scheme, the vectors $\mathbf{U}^{n+1}$ and $\mathbf{U}^\star$ must have the same mean value on each element.

We then compute the mean values of the physical variables, $\overline{\rho}_K^\star, \overline{u}_K^\star, \overline{v}_K^\star, \overline{p}_K^\star$ (the mean value $\overline{\rho}_K^\star$ of the density has already been calculated).

For pressure we also take the arithmetic mean of p at the vertices of K.

In contrast, the mean value of the velocity components u, v are defined by

$$\overline{u}_K^\star = \frac{\overline{(\rho u)}_K^\star}{\overline{\rho}_K^\star} \, , \quad \overline{v}_K^\star = \frac{\overline{(\rho v)}_K^\star}{\overline{\rho}_K^\star} \, . \tag{5.1}$$

For the components of momentum at time t^{n+1}, we will use the following value

$$\overline{(\rho u)}_K^{n+1} = \frac{1}{nv(K)} \sum_{i=1}^{nv(K)} \rho_{K,A_i}^{n+1} u_{K,A_i}^{n+1} \, , \quad \overline{(\rho v)}_K^{n+1} = \frac{1}{nv(K)} \sum_{i=1}^{nv(K)} \rho_{K,A_i}^{n+1} v_{K,A_i}^{n+1} . \tag{5.2}$$

Observe that these values are different from $\overline{u}_K^\star$, $\overline{v}_K^\star$, as they use the nodal values of density and velocity instead of those of the momentum.

Formulas (5.1)-(5.2) have been chosen to ensure existence and uniqueness of the solution of the minimisation problems to be defined below.

For every node A of the grid we compute the minimum and maximum of the mean values of the physical variables in the elements sharing node A :

$$w_{min}(A) = \min_{K \in T(A)} \overline{w}_K^\star, \quad w_{max}(A) = \max_{K \in T(A)} \overline{w}_K^\star, \quad \text{for} \quad w = \rho, u, v, p \tag{5.3}$$

The slopes of the physical variables ρ, u, v, p will be limited, in this order, in the following way. Let P denote the vector $(\rho, u, v, p)^T$ of physical variables.

In each element K with vertices A_i $(i = 1, \ldots, nv(K))$, $V_{|K}^{n+1}$ is defined by :

$$\begin{cases}
(i) \quad \overline{w}_K^{n+1} = \overline{w}_K^\star, \quad \text{for} \quad w = \rho, \, p, \text{ and } \overline{(\rho w)}_K^{n+1} = \overline{(\rho w)}_K^\star, \text{ for } w = u, \, v, \\[3mm]
(ii) \quad \text{For } i = 1, \ldots, nv(K), \, w = \rho, \, u, \, v, \, p : \\[2mm]
\qquad (1 - \alpha)\overline{w}_K^\star + \alpha w_{min}(A) \leq w_{K,A_i}^{n+1} \leq (1 - \alpha)\overline{w}_K^\star + \alpha w_{max}(A) \, , \; 0 \leq \alpha \leq 1, \\[3mm]
(iii) \quad \text{For } w = \rho, u, v, p \text{ the distance in } \mathbb{R}^3 \text{ between } w^{n+1} = (w_{K,A_i}^{n+1})_{i=1,\ldots,nv(K)} \\[2mm]
\qquad \text{and } w^\star = (w_{K,A_i}^\star)_{i=1,\ldots,nv(K)} \text{ is minimum .}
\end{cases}$$

The computation of $P_{|K}^{n+1}$ from $P_{|K}^\star$ thus amounts to four projection problems in $\mathbb{R}^{nv(K)}$ (one for each physical variable); as (i) defines a plane, and (ii) a cube, we look for the projection, on their intersection, of the corresponding variable $w^\star = (w_{K,A_i}^\star)_{i=1,\ldots,nv(K)}$.

Condition (i) allows for mass conservation, (ii) limits the variation of $\rho, \, u, \, v, \, p$ (in that order), and (iii) guarantees uniqueness of the solution.

After computing the vector of physical variables $P^{n+1} = \begin{pmatrix} \rho^{n+1} \\ u^{n+1} \\ v^{n+1} \\ p^{n+1} \end{pmatrix}$ we return to the conserva-

tive variables according to

$$
\mathbf{U}^{n+1} = \begin{pmatrix} \rho^{n+1} \\ \rho^{n+1} u^{n+1} \\ \rho^{n+1} v^{n+1} \\ \frac{p^{n+1}}{(\gamma-1)} + \frac{1}{2}\rho^{n+1}\left[\left(u^{n+1}\right)^2 + \left(v^{n+1}\right)^2\right] \end{pmatrix}.
$$

The slope limitation therefore requires the solution of a series of local minimization problems in 3 dimensional space, with the constraints (i) and (ii).

These projection problems can easily be solved by duality, as shown in [1].

In order to ensure the existence of a solution for the projection problems, we have to make sure that the intersection of the corresponding plane and cube is not empty. For density and pressure, it is easily seen that if we let $\rho_{K,A_i}^{n+1} = \overline{\rho}_K^\star$ and $p_{K,A_i}^{n+1} = \overline{p}_K^\star$ for $i = 1, 2, 3$, conditions (i) and (ii) are then satisfied, so that the relevant intersection is not empty.

As regards the velocity components, we can easily check, applying definitions (5.1) and (5.2), that if we let $u_{K,A_i}^{n+1} = \overline{u}_K^\star$ $(i = 1, \ldots, nv(K))$, then

$$
\overline{(\rho u)}_K^{n+1} = \frac{1}{nv(K)} \sum_{i=1}^{3} \rho_{K,A_i}^{n+1} \overline{u}_K^\star = \frac{1}{nv(K)} \left(\sum_{i=1}^{nv(K)} \rho_{K,A_i}^{n+1} \right) \frac{\overline{(\rho u)}_K^\star}{\overline{\rho}_K^\star}
$$

$$
= \overline{(\rho u)}_K^\star .
$$

with a similar result for the second velocity component.

The parameter α controls the extent of the slope limitation process. For $\alpha = 0$, we get the most stringent limitation: the solution P^{n+1} (and therefore $\mathbf{U}^{n+1}$) is piecewise constant, thus reducing the method to the usual (spatially) first order accurate scheme.

In our numerical experiments, we have usually chosen $\alpha = 0.5$, a value which led to optimal results in the scalar case (cf. [18]).

For one-dimensional problems, the limitation procedure reduces to the usual van Leer solpe limitation ([21]).

6. The numerical algorithm

The above description of the discontinuous finite element method can be summarized within the frame of a two-step scheme.

Assuming for simplicity that we use an explicit Euler time discretization, let $\mathbf{U}^n \in W^4$ be the solution obtained at time $t = t^n$. In the first step (predictor), we compute an approximation $\mathbf{U}^\star \in W^4$ of the solution at time t^{n+1}. This predictor step consists in a finite element calculation, but features the use of Riemann solvers.

In the second step, which can be viewed as a correction step, we limit the vector $\mathbf{U}^\star$ to obtain an approximate solution $\mathbf{U}^{n+1}$.

6.1. First order in time discretization:
1 - Predictor step : Finite element calculation

$$
\begin{cases}
\text{Compute } \mathbf{U}^\star \in W^4 \text{ such that} \\[2mm]
\displaystyle\int_{K_i} \frac{\mathbf{U}^\star - \mathbf{U}^n}{\Delta t^n} \varphi_{j,i}\, dS = \int_{K_i} \left(\mathbf{f}_1(U^n)\frac{\partial \varphi_{j,i}}{\partial x} + \mathbf{f}_2(U^n)\frac{\partial \varphi_{j,i}}{\partial y} \right) dS - \int_{\partial K_i} (\mathbf{f}(\mathbf{U}^n) \cdot n)\, \varphi_{j,i}\, d\sigma \\[2mm]
\text{for each } K_i \in \mathcal{T}_h \text{ and } \varphi_{l,i}(l = 1,\dots, nv(K))
\end{cases}
\tag{6.1}
$$

2 - Limitation step

This step limits the variation range of components of the vector of physical variables $\begin{pmatrix} \rho^\star \\ u^\star \\ v^\star \\ p^\star \end{pmatrix}$

obtained in the predictor step. It leads to $\mathbf{U}^{n+1}$, the final approximation of the vector of conservative variables at time t^{n+1}.

6.2. Second order in time discretization:
1 - Predictor step at $n + \frac{1}{2}$: Finite element calculation

$$
\begin{cases}
\text{Compute } \mathbf{U}^{n+\frac{1}{2}} \in W^4 \text{ such that} \\[2mm]
\displaystyle\int_{K_i} \frac{\mathbf{U}^{n+\frac{1}{2}} - \mathbf{U}^n}{\frac{\Delta t^n}{2}} \varphi_{j,i}\, dS = \int_{K_i} \left(\mathbf{f}_1(U^n)\frac{\partial \varphi_{j,i}}{\partial x} + \mathbf{f}_2(U^n)\frac{\partial \varphi_{j,i}}{\partial y} \right) dS - \int_{\partial K_i} (\mathbf{f}(\mathbf{U}^n) \cdot n)\, \varphi_{j,i}\, d\sigma \\[2mm]
\text{for each } K_i \in \mathcal{T}_h \text{ and } \varphi_{l,i}(l = 1,\dots, nv(K))
\end{cases}
$$

$$\tag{6.2}$$

2 - Predictor step at $n + 1$: Finite element calculation

$$
\begin{cases}
\text{Compute } \mathbf{U}^\star \in W^4 \text{ such that} \\[2mm]
\displaystyle\int_{K_i} \frac{\mathbf{U}^\star - \mathbf{U}^n}{\Delta t^n} \varphi_{j,i}\, dS = \int_{K_i} \left(\mathbf{f}_1(U^{n+\frac{1}{2}})\frac{\partial \varphi_{j,i}}{\partial x} + \mathbf{f}_2(U^{n+\frac{1}{2}})\frac{\partial \varphi_{j,i}}{\partial y} \right) dS - \int_{\partial K_i} \left(\mathbf{f}(\mathbf{U}^{n+\frac{1}{2}}) \cdot n\right) \varphi_{j,i}\, d\sigma \\[2mm]
\text{for each } K_i \in \mathcal{T}_h \text{ and } \varphi_{l,i}(l = 1,\dots, nv(K))
\end{cases}
$$

$$\tag{6.3}$$

3 - Limitation step

This step limits the variation range of components of the vector of physical variables $\begin{pmatrix} \rho^\star \\ u^\star \\ v^\star \\ p^\star \end{pmatrix}$

obtained in the predictor step. It leads to $\mathbf{U}^{n+1}$, the final approximation of the vector of conservative variables at time t^{n+1}.

We observe that the two steps are independent from each other, and the limitation process is distinct from the flux calculation, contributing to the originality of the method.

7. Numerical experiments

7.1. Shock reflexion problem. This is a standard test problem and has been widely discussed in Colella ([10]) and in Peraire et al ([28]). The problem definition is given in Fig. (4).

The boundary conditions

- On $\Gamma_{Wall} = \Gamma_B$, the slip condition is imposed.

$$V \cdot n = 0, \tag{7.1}$$

with $V = \begin{pmatrix} u \\ v \end{pmatrix}$ is the flow velocity and $n \in \mathbb{R}^2$ is the outgoing normal vector to Γ_W.
- On Γ_∞, there are two types of borders: $\Gamma_\infty = \Gamma_\infty^1 \cup \Gamma_\infty^2$.
  It is assumed the the flow is uniform on each of the two boundaries Γ_∞^1 et Γ_∞^2.

- On Γ_∞^1, $U_\infty^1 = \begin{pmatrix} \rho_1 \\ \rho_1 V_1 \\ \dfrac{p_1}{(\gamma - 1)} + \dfrac{1}{2}\rho_1 \| V_1 \|^2 \end{pmatrix}$, with $\begin{cases} \rho_1 = 1.0 \\ V_1 = \begin{pmatrix} 2.9 \\ 0.0 \end{pmatrix} \\ p_1 = 0.714 \end{cases}$

- On Γ_∞^2, $U_\infty^2 = \begin{pmatrix} \rho_2 \\ \rho_2 V_2 \\ \dfrac{p_2}{(\gamma - 1)} + \dfrac{1}{2}\rho_2 \| V_2 \|^2 \end{pmatrix}$, with $\begin{cases} \rho_2 = 1.7 \\ V_2 = \begin{pmatrix} 2.618 \\ -0.506 \end{pmatrix} \\ p_2 = 1.528 \end{cases}$

- On $\Gamma_{exit} = \Gamma_S$, the flow is free.

Now we describe how these boundary conditions are implemented. Let $\mathcal{A}$ a boundary edge and K a boundary element which $\mathcal{A}$ is an edge. We note $\mathbf{U}_l$ the left state defined in K. A fictious element is introduced adjacent to K and outside the domain in which the the state in noted $\mathbf{U}_r$. The definition of this state depends on the boundary condition.
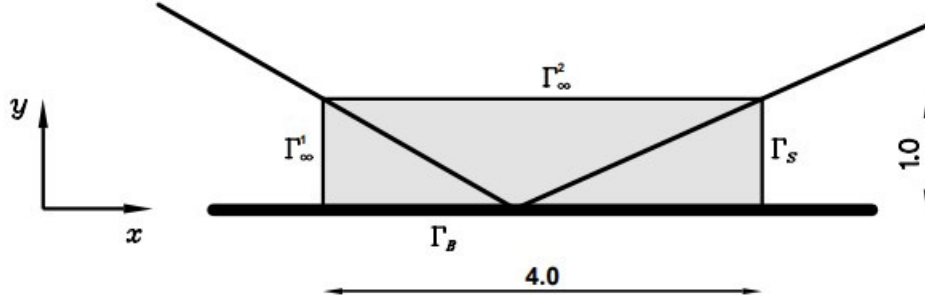
FIGURE 4. Regular shock reflection at a wall: the problem definition and the computational domain (shaded)

● On $\Gamma_{Wall} = \Gamma_B$, the state $\mathbf{U}_r$ is defined by the following three conditions:

$$
\left\{
\begin{array}{l}
(i) \quad \rho_r = \rho_l \\[2ex]
(ii) \quad \mathbf{V}_r = \begin{pmatrix} u_r \\ v_r \end{pmatrix} \text{ is the symmetric of } \mathbf{V}_l = \begin{pmatrix} u_l \\ v_l \end{pmatrix} \\[2ex]
\qquad \text{with respect to the edge } \mathcal{A}. \\[2ex]
(iii) \quad p_r = p_l
\end{array}
\right.
$$

Note that the relationship (7.1) is satisfied thanks to the condition (ii).
● On Γ_∞ the state U_r is equal to the state imposed at infinity:

$$U_r = U_\infty^1 \quad \text{sur } \Gamma_\infty^1$$
$$U_r = U_\infty^2 \quad \text{sur } \Gamma_\infty^2$$

The numerical fluxes on the boundary edges $\widetilde{F}_\mathcal{A}(U_l, U_r)$ are then calculated in the normal direction n of the same way for internal edges using $\mathbf{U}_l$ and $\mathbf{U}_r$ defined above.

The algorithm for computing the stationary solution is initiated by the state $\mathbf{U}_\infty^1$.

The exact solution to this problem is an incoming shock of 29 degrees with lower and a reflected shock of 23.28 degrees. The exact solution past the second shock should be $\rho = 2.68732, u = 2.40148, v = 0, p = 2.93413$

Figures (6), (7) and (8) show the pressure contour computed with an anisotropic refinement using entropy stable scheme, Roe scheme and Osher Scheme. Notice how the incident shock and the reflected one are approximated much better. This is due to the fact that the triangles are partially aligned with the incident and reflected shock.

This test problem is simple in structure: three constant values separated by two shocks. We use it to test

- the nonoscillatory property of our multi-dimentional slope limiter
- the behavior of numerical reflecting boundary at the lower boundary, and
- the effect when triangles are aligned with shocks.

TABLE 1. CPU of the simulations

D.F.E. Scheme ($P^1 1$)	CPU time (s)
Roe	36.66
Osher	34.12
Ess	56.17

Fig.(9) shows the convergence fistory of residual for the D.F.E. using entropy stable scheme. We used two schemes for time integration one in order one (6.1) and the other in order two in time (6.2).

Entropy stable scheme, Roe scheme and Osher scheme give almost identical results, and are able to preserve the positivity of density and pressure, as seen in Fig. (10).

Remark 3. *(CPU times of the simulations). The simulations performed for shock reflection problem are reported in Table 1, Entropy stable scheme is about* 20% *more expensive.This cost due to the construction of the conservative entropy flux.*
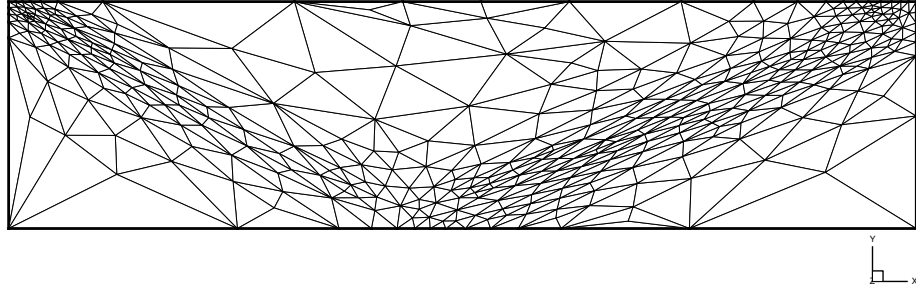
FIGURE 5. Computational grids for regular shock reflection at a wall test case, triangular mesh, 356 vertices, 663 triangles

PRESSURE: 0.80 0.82 1.00 1.12 1.20 1.37 1.40 2.12 2.33 2.61 2.73 2.80 2.83 2.88 2.89
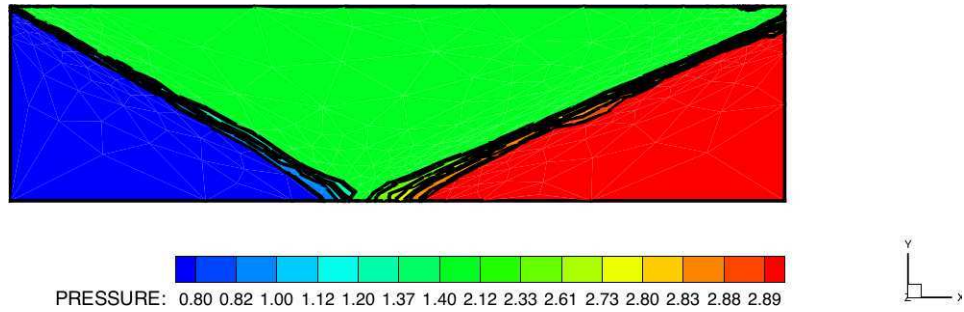
FIGURE 6. P^1 solution (pressure contours) using entropy stable scheme

A study of computational accuracy for the shock reflexion problem is presented with the use of the L^1 norm. Table 2 shows the L^1 error and the convergence rate δ are calculated as follows:
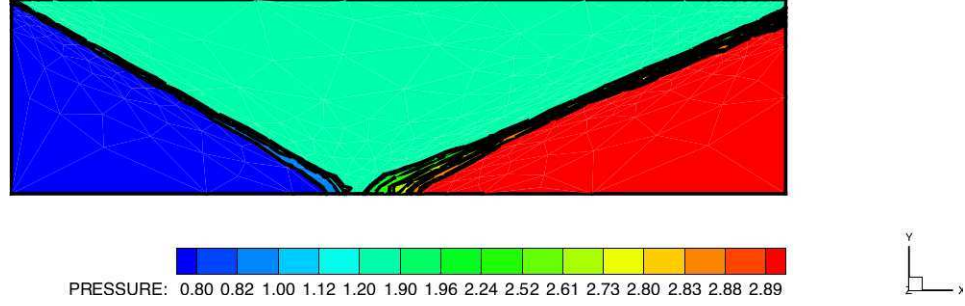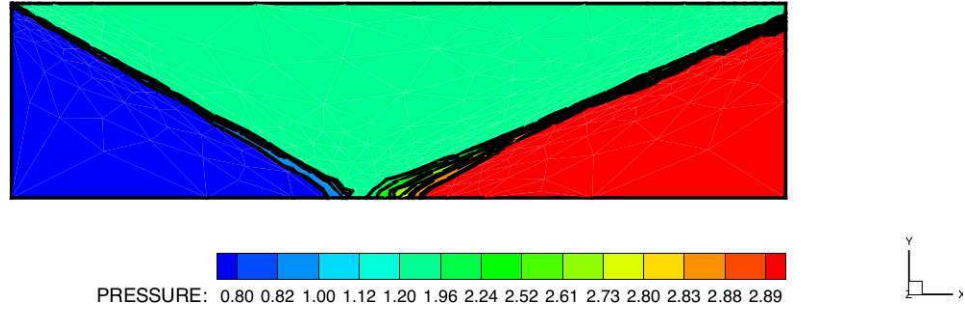
FIGURE 7. P^1 solution (pressure contours) using Roe scheme

FIGURE 8. P^1 solution (pressure contours) using Osher scheme

TABLE 2. Convergence result for Euler equation, discontinuous initial data

		constant approximation (P^0)		linear approximation (P^1)	
Grid	Number of cells	$\| \rho_{exact} - \rho_h \|_{L^1}$	δ	$\| \rho_{exact} - \rho_h \|_{L^1}$	δ
Coarse	663	0.0261		0.0124	
Medium	4589	0.0135	0.94	0.0061	1.00
Fine	9383	0.0063	1.08	0.0024	1.36

$e(h) = \| \rho_{exact} - \rho_h \|_{L^1}$ and $\delta = \dfrac{ln\left(\frac{e(h_1)}{e(h_2)}\right)}{ln\left(\frac{h_1}{h_2}\right)}$ We observe that the errors obtained with the

piecewise linear approximation (P^1) are significantly smaller than with piecewise constants (P^0). However, the rate of convergence is not improved, which can be improved by considering implicit scheme in a forthcoming paper.

7.2. Flow around a double ellipse. This test case was proposed in the workshop "Hypersonic Flows For Reentry Problems" [19]. The domain of computation Ω and its boundaries ($\Gamma_{Wall} = \Gamma_B$), (Γ_∞) and ($\Gamma_{Exit} = \Gamma_S = \Gamma_S^1 \cup \Gamma_S^2$) are shown in Fig. (1).
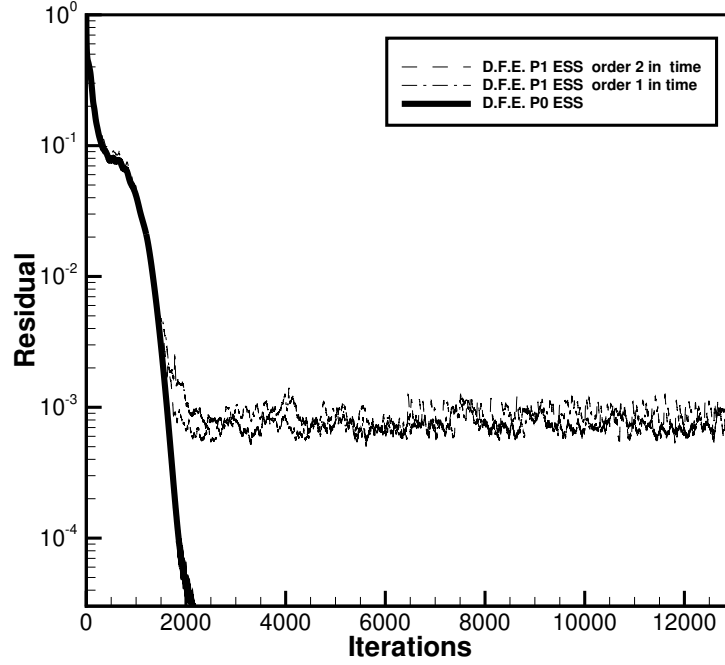
The boundary conditions

FIGURE 9.   Convergence history of residual of shock reflection problem using entropy stable scheme (ESS)

- On $\Gamma_{Wall} = \Gamma_B$, the slip condition is imposed $\boldsymbol{V} \cdot \boldsymbol{n} = 0$, and was implemented in same way as in the previous problem.
- On Γ_∞, we will suppose that the flow is uniform (the velocity inflow $\boldsymbol{V}_\infty$ normalized to unity).

$$\rho_\infty = 1, \ \ \boldsymbol{V}_\infty = \begin{pmatrix} cos\ \alpha \\ sin\ \alpha \end{pmatrix}, \ \ p_\infty = \frac{1}{\gamma M_\infty^2} \tag{7.2}$$

    where α is the angle of incidence and M_∞ means the Mach number at infinity.
- On Γ_S, the flow is free. the condition is also implemented in the same way as in the previous problem.

In this problem the stationary solution in initiated by the state $\mathbf{U}_\infty$

$$\mathbf{U}_\infty = \begin{pmatrix} \rho_\infty \\ \rho_\infty \boldsymbol{V}_\infty \\ \dfrac{p_\infty}{(\gamma - 1)} + \dfrac{1}{2}\rho_\infty \, \|\boldsymbol{V}_\infty\|^2 \end{pmatrix},$$

where ρ_∞, p_∞ and $\boldsymbol{V}_\infty$ are given by (7.2).
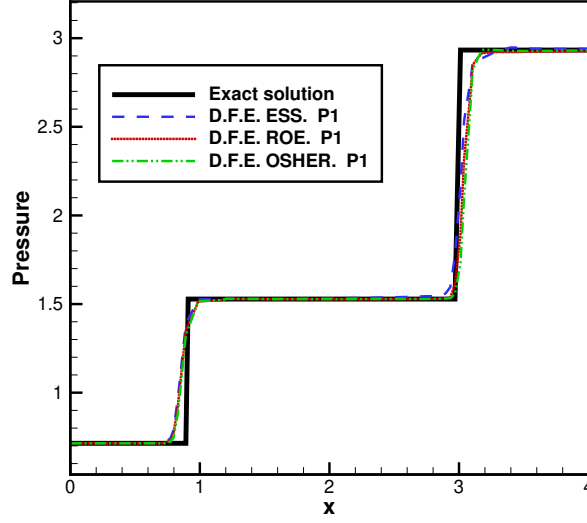
D.G. P^1

FIGURE 10. Pressure distribution at $y = 0.525$, Entropy stable, Roe and Osher schemes

The numerical values defining the tests are: $\alpha = 30^o$, $\gamma = 1.4$, $M_\infty = 8.15$ The results obtained with the discontinuous finite element method as described above and compared with Roe scheme.

We present results obtained on quadrangular meshes shown in Fig. (11). All comparisons where made on the mesh shown in Fig. (11). Results for mach contours are streamlines shown in Figs. (13) and (12). All Riemann solvers are good enough, the solutions are better, except at the stagnation point, Roe scheme shows instability, see Fig. (12). This instability can be highlighted in Fig. (12) compared to entropy stable scheme see Fig. (13).

Fig. (14) shows pressure coefficient along the wall comparing Roe and Entropy stables schemes for second order D.G. method. One observe that results obtained with quadrangular meshes are similar except at the stagnation point.

8. Conclusion and perspectives

In this paper, we consider systems of conservation laws in two space dimensions and propose a discontinuous finite element method associated to a slop limitation to construct an accurate method. The method is based on the following ingredients,

- The entropy variables (rather than the conservative variables) serve as the degrees of freedom.
- The (spatial) numerical flux function is identical to the entropy stable fluxes (entropy conservative fluxes + numerical diffusion operators) proposed recently in the context of high-resolution finite volume schemes on unstructured grids, [25, 26] and references therein.
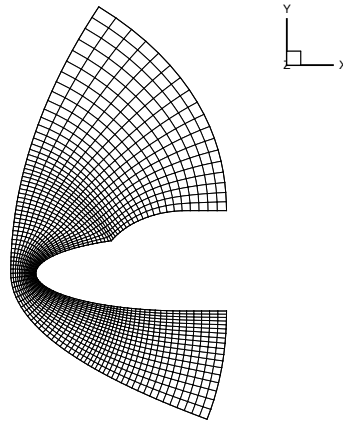
FIGURE 11. Computational grids for double ellipse test case, quadrangular mesh, 1729 vertices, 1620 quadrangles
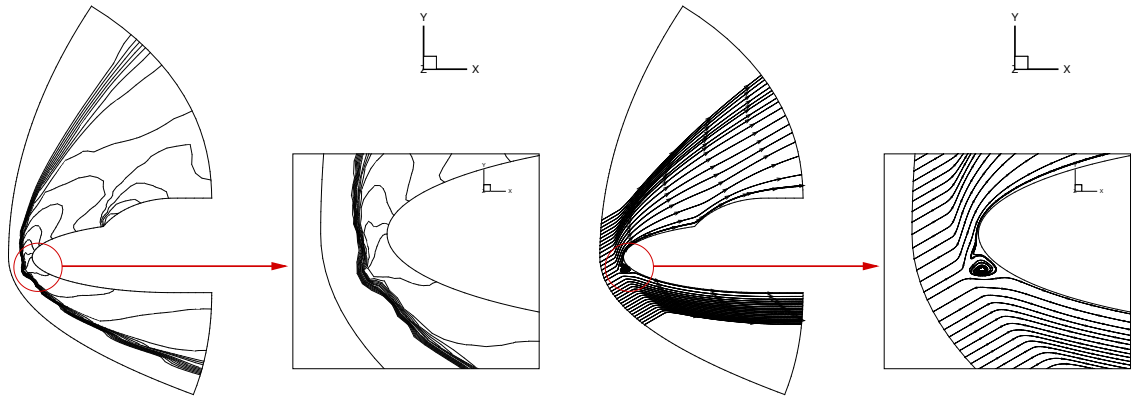

FIGURE 12. Q^1 solution (Mach contours and Streamlines) using Roe scheme

- For each time step the slope limitation is introduced as a separate step performed after finite element calculation.

The resulting schemes are shown

- To compute discontinuities like shocks and contact discontinuities robustly and there have been no observed anomalies on structured grids, but on poor quality unstructured grids the carbuncle phenomena returns.

Also we have observed some convergence difficulties showing that it is necessary to improve upon our present local time stepping (Euler explicit). The design of an implicit scheme is considered in a forthcoming paper.
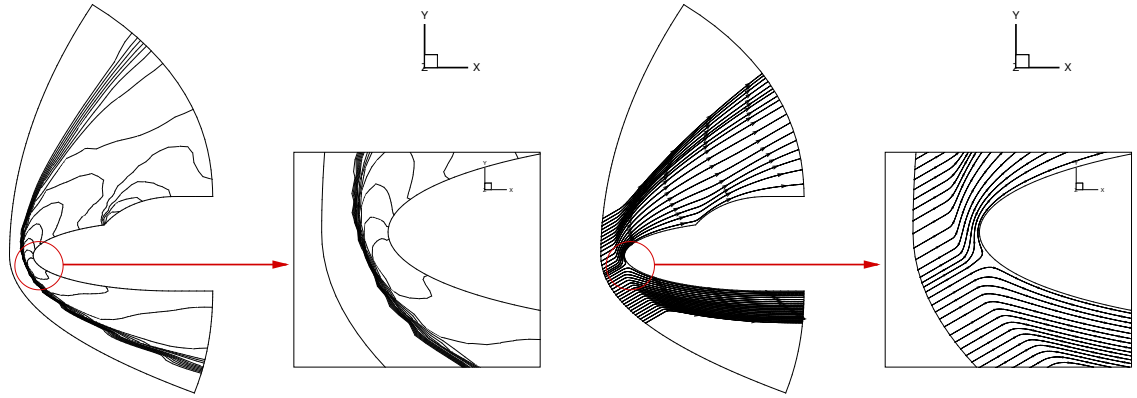
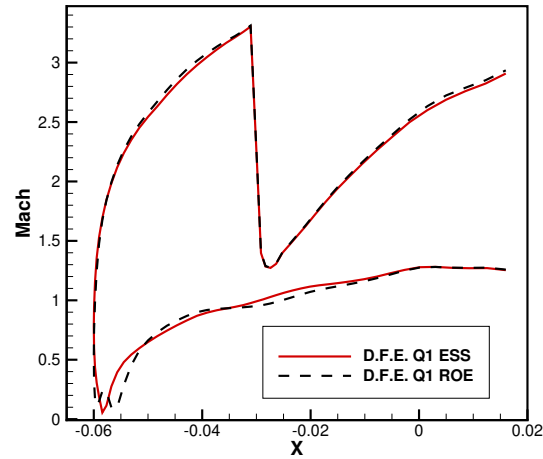FIGURE 13. Q^1 solution (Mach contours and Streamlines) using entropy stable scheme

FIGURE 14. Mach distribution along the inviscid wall, Entropy stable vs. Roe schemes

Acknowledgement

References

[1] P. Arminjon, M.C. Viallon, A. Madrane and H. Kaddouri, Discontinuous finite elements and a 2-dimensional finite volume generalization of the Lax-Friedrichs and Nessyahu-Tadmor schemes for compressible flows on unstructured grids, CFD Review, M. Hafez and K. Oshima, editors, John Wiley, pp. 241–261, (1997).

[2] T.J. Barth, Numerical methods for gaz-dynamics systems on unstructured meshes. In An introduction to Recent Developments in Theory and Numerics of Conservation Laws pp 195-285. Lecture Notes in Computational Science and Engineering Volume 5, Springer, Berlin. Eds D. Kroner, M. Ohlberger and Rohde, C., (1999).

[3] M. W. Bohm, A. R. Winters, G. J. Gassner, D. Derigs, F. J. Hindenlang and J. Saur. An entropy stable nodal discontinuous Galerkin method for the resistive MHD equations. Part I: Theory and numerical verification. Journal of Computational Physics, to appear. DOI: 10.1016/j.jcp.2018.06.027.

[4] M. H. Carpenter, T. C. Fisher, E. J. Nielsen and S. H. Frankel. Entropy stable spectral collocation schemes for the NavierStokes equations: discontinuous interfaces. SIAM Journal on Scientific Computing, 36:B835B867, 2014.

[5] T. Chen and C.-W. Shu. Entropy stable high order discontinuous Galerkin methods with suitable quadrature rules for hyperbolic conservation laws. Journal of Computational Physics, 345:427461, 2017.

[6] G. Chavent and J. Jaffré and R. Eymard and D. Guérillot and L. Weill, Discontinuous and mixed finite elements for two-phase incompressible flow, SPE Reservoir Engineering, 5, 567–575, (1990).

[7] G. Chavent and J. Jaffré, Mathematical Models and Finite Element for Reservoir Simulation ", "North Holland, Amsterdam, (1986).

[8] B. Cockburn, S. Hou and C.W. Shu, The Runge-Kutta local projection discontinuous Galerkin Finite Element Method for conservation laws IV : the multi-dimensional case, Math. Comp. Vol. 54, No. 190. 545–581, (1990).

[9] Cockburn, B., Lin, S-y, Shu, C.-W., TVB Runge-Kutta local projection discontinuous Galerkin finite element method for conservation laws. III. One-dimensional systems. J. Comput. Phys. 84, 90–113, (1989).

[10] P. Collela, Multi-dimensional upwind methods for hyperbolic conservation laws, J. Comput. Physics, 87, 171–200, (1990).

[11] C. Dafrmos, Hyperbolic Conservation Laws in Continuum Physics. Springer, Berlin, (2000).

[12] J.-A. Désidéri and A. Dervieux, Compressible flow solvers using unstructured grids. In Computational fluid dynamics, Vol. 1, 2, volume 88 of von Karman Inst. Fluid Dynam. Lecture Ser., page 115. von Karman Inst. Fluid Dynamics, Rhode-St- Gense, (1988).

[13] U.S. Fjordholm, S. Mishra and E. Tadmor, Energy preserving and energy stable schemes for the shallow water equations. "Foundations of Computational Mathematics", Proc. FoCM held in Hong Kong 2008 (F. Cuckers, A. Pinkus and M. Todd, eds), London Math. Soc. Lecture Notes Ser. 363, pp. 93–139, (2009).

[14] Fjordholm, U.S., Mishra, S., Tadmor, E., Arbitrary order accurate essentially non-oscillatory entropy stable schemes for systems of conservation laws. SIAM J. Numer. Anal. 50(2), 544–573, (2012).

[15] G. J. Gassner, A. R. Winters, F. J. Hindenlang, and D. A. Kopriva. The BR1 scheme is stable for the compressible NavierStokes equations. Journal of Scientific Computing, 77:154200, 2018.

[16] Harten, A., Engquist, B., Osher, S., Chakravarty, S.R., Uniformly high order accurate essentially nonoscillatory schemes, III. J. Comput. Phys. 71, 231–303, (1987).

[17] E. Godlewski and P.-A. Raviart, Numerical approximation of hyperbolic systems of conservation laws, volume 118 of Applied Mathematical Sciences. Springer-Verlag, New York, (1996).

[18] G.D.V. Gowda, Discontinuous finite element for nonlinear scalar conservation laws, Thèse de Doctorat, Université Paris IX-Dauphine, (1988).

[19] INRIA and GAMNI-SMAI, Workshop on hypersonic flows for reentry problems, Problem 6 : Flow over a double ellipse, test case 6.1 : Non-Reactive Flows. Antibes, France, January 22-25, (1990)

[20] F. Ismail and P. L. Roe, Affordable, entropy-consistent Euler flux functions II: Entropy production at shocks. J. Comput. Phys., vol. 228, issue 15, pp. 5410–5436, (2009).

[21] B.V. Leer, Towards the ultimate conservative scheme: IV. A new approach to numerical convection, J. Comput. Physics, 23, 276–299, (1977).

[22] P. Lesaint and P. Raviart, On a finite element method for solving the neutron transport equations, in Mathematical Aspects of Finite Elements in Partial Differential Equations, Academic Press, New York, (1974).

[23] Y. Liu, C.-W. Shu and M. Zhang. Entropy stable high order discontinuous Galerkin methods for ideal compressible MHD on structured meshes. Journal of Computational Physics, 354:163178, 2018.

[24] A. Madrane, E.Tadmor, Entropy stability of Roe-type upwind finite volume methods on unstructured grids, in Hyperbolic Problems: Theory, Numerics, Applications, Proceedings of the 12th International Conference in

2008, Vol. 67(2) (E. Tadmor, J.-G. Liu and A. Tzavaras, eds), AMS Proc. Symp. Applied Math., University of Marylan, 775–784, (2009).

[25] A. Madrane, U. S. Fjordholm, S. Mishra, E. Tadmor, Entropy conservative and entropy stable finite volume schemes for multi-dimensional conservation laws on unstructured meshes, ECCOMAS 2012, Proc. J. Eberhard-steiner et al. (eds.), Vienna, Austria, September 10-14, (2012).

[26] A. Madrane, S. Mishra, E. Tadmor, Entropy conservative and entropy stable finite volume/finite element schemes for the Navier-Stokes equations on unstructured meshes, ECCOMAS 2014, Proc. E. Onãte et al. (eds.), Barcelona Spain, Jul. 20, (2014).

[27] S. Osher and F. Salomon, Upwind difference schemes for hyperbolic systems of conservation laws, Mathematics of Computation, 38, 158, 339–374, (1982).

[28] J. Peraire and M. Vahdati and K. Morgan and O.C. Zienkiewicz, Adaptive remeshing for compressible flow computations, J. Comput. Physics, 72, 449–466, (1987).

[29] J. Peraire and L. Formaggia and J. Peiro and K. Morgan and O. C. Zienkiewicz, Finite element Euler computation in three dimensions, AIAA paper, 87-0032, (1987).

[30] W. Reed and T. Hill, Triangular mesh methods for the neutron transport equation, Tech.Rep. LA-UR-73-479, Los Alamos Scientific Laboratory, (1973).

[31] F. Renac. Entropy stable DGSEM for nonlinear hyperbolic systems in nonconservative form with application to two-phase flows. Journal of Computational Physics, 382:126, 2019.

[32] P. L Roe, Approximate Riemann Solvers, Parameter Vectors, and Difference Schemes, Journal of Computational Physics, 43, 357–372, (1981).

[33] Shu, C.W., Osher, S., Efficient implementation of essentially non-oscillatory schemesII. J. Comput. Phys. 83, 32–78, (1989).

[34] Z. Sun, J. A. Carillo and C.-W. Shu. A discontinuous Galerkin method for nonlinear parabolic equations and gradient flow problems with interaction potentials. Journal of Computational Physics, 352:76104, 2018.

[35] Z. Sun, J. A. Carillo and C.-W. Shu. An entropy stable high-order discontinuous Galerkin method for cross-diffusion gradient flow systems. Kinetic and Related Models, 12:885908, 2019.

[36] E. Tadmor, The numerical viscosity of entropy stable schemes for systems of conservation laws, I. Math. Comp., 49, 91–103, (1987).

[37] E. Tadmor, Entropy stability theory for difference approximations of nonlinear conservation laws and related time–dependant problem, Acta Numer., 12, 451–512, (2003).